

# Electronic Structure and Transport in Graphene/Haeckelite Hybrids: An *Ab Initio* Study

Zhen Zhu, Zacharias G. Fthenakis and David Tománek

Physics and Astronomy Department, Michigan State University, East Lansing, Michigan 48824, USA

E-mail: tomanek@pa.msu.edu

PACS numbers: 73.40.-c, 61.48.Gh, 73.22.Pr, 73.22.-f

**Abstract.** We combine *ab initio* density functional theory (DFT) structural studies with DFT-based nonequilibrium Green function calculations to investigate how the presence of non-hexagonal rings affects electronic transport in graphitic structures. We find that infinite monolayers, finite-width nanoribbons and nanotubes formed of 5-8 haeckelite with only 5- and 8-membered rings are generally more conductive than their graphene-based counterparts. Presence of haeckelite defect lines in the perfect graphitic structure, a model of grain boundaries in CVD-grown graphene, increases the electronic conductivity and renders it highly anisotropic.

*Keywords:* graphene, haeckelite, hybrid structure, charge transport, DFT

## 1. Introduction

Graphene is a unique 2D material that combines extraordinarily high electrical and thermal conductivity [1, 2] with mechanical strength, flexibility, thermal and chemical stability. Interest in this system increased significantly after a successful mechanical exfoliation using a Scotch tape has been reported [3] that yielded large, defect-free samples. As a scalable alternative to the “Scotch tape” exfoliation technique, chemical vapor deposition (CVD) is commonly being used now to form graphene monolayers on metal substrates including Cu [4, 5, 6, 7]. The quality of CVD-grown films is inferior to those produced by exfoliation, since gas phase deposition leads to simultaneous growth of graphene flakes that eventually interconnect, forming grain boundaries with a defective, haeckelite-like structure [8, 9, 10, 11, 12, 13] consisting of non-hexagonal carbon rings [14]. Pure haeckelite structures and their hybrids with graphene have a significantly lower thermal conductivity than pure graphene [15]. Only few theoretical studies have investigated electronic transport in selected graphitic carbon nanostructures with non-hexagonal rings including hybrid graphene-haeckelite structures [16, 17] and haeckelite nanotubes [18, 19, 20]

Here we combine *ab initio* density functional theory (DFT) structural studies with DFT-based nonequilibrium Green function calculations to investigate how the presence of non-hexagonal rings affects electronic transport in graphitic structures. We find that infinite monolayers, finite-width nanoribbons and nanotubes formed of 5-8 haeckelite with only 5- and 8-membered rings are generally more conductive than their graphene-based counterparts. Presence of haeckelite defect lines in the perfect graphitic structure, a model of grain boundaries in CVD-grown graphene, increases the electronic conductivity and renders it highly anisotropic.

Haeckelites [8, 9, 10, 11, 12, 13] consist of periodic 2D arrangements of non-hexagonal rings of  $sp^2$  bonded carbon atoms. Even though these structures have not been synthesized yet on a large scale, similar atomic arrangements have been observed (*i*) in 5-7 and 5-8 defect lines forming the in-plane interface between adjacent graphene flakes [14, 21, 22], (*ii*) in a vitreous atomic network formed during electron-beam irradiation of graphene [23], and (*iii*) in 5-7 ring structures filling graphene nanoholes during the healing process of these defects [24]. Most theoretical studies have focused on the equilibrium structure, stability and growth stability of haeckelites [8, 9, 10, 11, 12, 13, 17, 25, 26, 27, 28, 29] and found these systems to be either metallic, semi-metallic or semiconducting [12, 13, 27].

With continuing interest in CVD-grown graphene as an electronic material, increased attention must be given to carrier scattering at haeckelite-like grain boundaries connecting defect-free graphene regions. The most plausible model geometry to investigate charge transport in polycrystalline graphene is that of interconnected strips of haeckelite and graphene. A consistent picture should be obtained by comparing the effect of different structural arrangements and widths of haeckelite and graphene strips on the conductance and its anisotropy. As a counterpart to transport studies in

graphene nanoribbons and nanotubes, we present corresponding results for haeckelite nanoribbons and nanotubes.

## 2. Methods

To gain insight into the equilibrium structure, stability and electronic properties of haeckelite structures, we performed DFT calculations as implemented in the SIESTA code [30]. Infinite 2D layers and 1D ribbons and nanotubes were separated by 10 Å thick vacuum regions in a 3D periodic arrangement. We used the Ceperley-Alder [31] exchange-correlation functional as parameterized by Perdew and Zunger [32], norm-conserving Troullier-Martins pseudopotentials [33], and a double- $\zeta$  basis including polarization orbitals. The reciprocal space was sampled by a fine grid [34] of at least  $8 \times 8 \times 1$   $k$ -points in the Brillouin zone of the 2D primitive unit cell and its equivalent for 1D structures or larger 2D supercells. We used a mesh cutoff energy of 180 Ry to determine the self-consistent charge density, which provided us with a precision in total energy of  $\lesssim 2$  meV/atom. All geometries have been optimized using the conjugate gradient method [35], until none of the residual Hellmann-Feynman forces exceeded  $10^{-2}$  eV/Å.

Electronic transport properties were investigated using the nonequilibrium Green's function (NEGF) approach as implemented in the TRAN-SIESTA code [36]. Ballistic transport calculations for optimized structures were performed using a single- $\zeta$  basis with polarization orbitals, a 180 Ry mesh cutoff energy, and the same  $k$ -point grid [34] as used for structure optimization.

## 3. Results and discussion

### 3.1. 5-8 haeckelite

A perfect 2D monolayer of 5-8 haeckelite containing only 5- and 8-membered rings is shown in Fig. 1(a). The optimum rectangular unit cell is spanned by the Bravais lattice vectors  $a_1=4.87$  Å in the  $x$ -direction and  $a_2=6.93$  Å in the  $y$ -direction. The 5-8 haeckelite structure is about 0.36 eV/atom less stable than graphene, which is comparable to the stability of narrow carbon nanotubes. Due to this relatively high stability, we expect 5-8 haeckelite structures to coexist with graphene at grain boundaries.

The electronic band structure of 5-8 haeckelite is presented in Fig. 1(b). In contrast to semimetallic graphene, 5-8 haeckelite is metallic and has a finite electronic density of states at the Fermi level. Whereas the Fermi surface of graphene consists of 6 isolated  $k$ -points, that of 5-8 haeckelite is a line of finite length that intersects the  $\Gamma$ -Y high-symmetry line, as seen in Fig. 1(b).

The results of our quantum transport calculation for this system are shown in Fig. 1(c). Besides the improved conductivity over graphene, suggested by the increased density of states at the Fermi level, we find the conductivity to be also anisotropic, as expected when considering the atomic arrangement in Fig. 1(a). We find the electrical

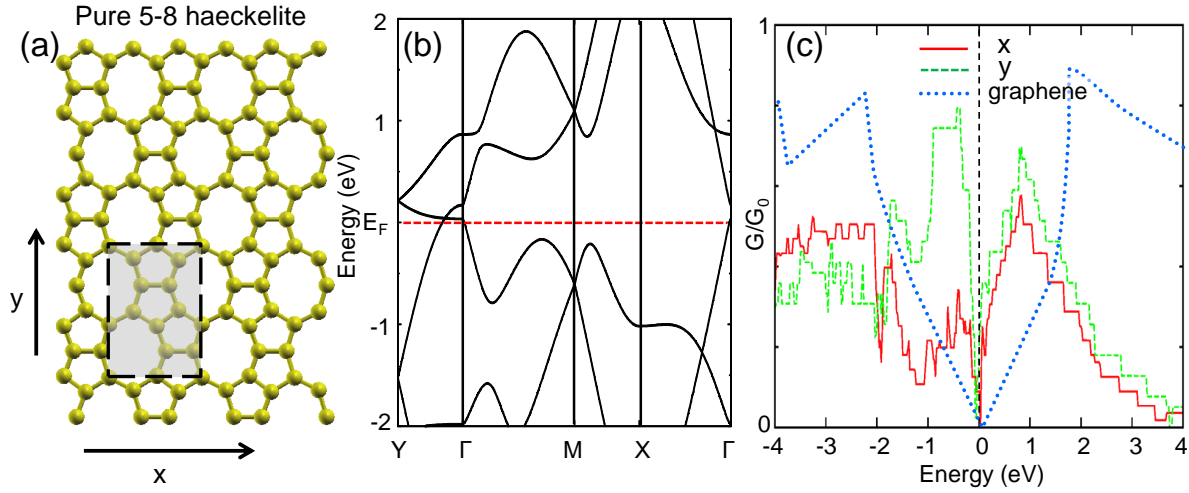


**Figure 1.** (Color online) (a) Atomic structure and (b) electronic band structure of 5-8 haeckelite with only 5- and 8-membered rings. The primitive unit cell is indicated by the shaded region. (c) Electronic conductance  $G/G_0$  along the horizontal  $x$ -direction, shown by the solid red line, and the vertical  $y$ -direction, shown by the dashed green line.  $G$  is normalized by the width of the unit cell normal to the transport direction.  $E = 0$  corresponds to carrier injection at  $E_F$ .

conductance along the  $y$  direction to be much higher than along the  $x$ -direction, and even observe a very narrow transport gap at  $E_F$ . These findings are consistent with a very anisotropic Fermi surface that crosses the  $\Gamma$ - $Y$ , but not the  $\Gamma$ - $X$  high-symmetry line in Fig. 1(b).

### 3.2. 5-8 haeckelite nanoribbons and nanotubes

Finite-width graphene nanoribbons and carbon nanotubes have received wide attention, since – unlike infinite graphene monolayers – some of these structures display sizeable band gaps. In analogy to these structures, we also studied quantum transport in 1D haeckelite nanoribbons (h-NRs) and nanotubes (h-NTs). In Fig. 2, we present our results for h-NRs with different widths  $W$  that are passivated by hydrogen at the edge. The atomic structure of the three narrowest haeckelite nanoribbons are shown in Figs. 2(a-c). We find the optimum lattice constant  $L \approx 4.9 \text{ \AA}$  to be nearly independent of the width  $W$ . We also note that structures in Fig. 2(a) and 2(c) have mirror symmetry, whereas that in Fig. 2(b) does not.

As seen in panels (d-i) of Fig. 2, we found the electronic structure and conductance of h-NRs to depend sensitively on the ribbon width. Structures with an odd number of 8-membered rings in the unit cell, depicted in Figs. 2(a) and 2(c), are narrow-gap semiconductors, with the fundamental band gap decreasing with increasing width from  $E_g = 0.05 \text{ eV}$  in Fig. 2(a,d) to  $E_g = 0.02 \text{ eV}$  in Fig. 2(c,f). Structures with an even number of 8-membered rings in the unit cell are all metallic. One example with two 8-membered rings in the unit cell is shown in Fig. 2(b,e). Quantum conductance  $G$  of

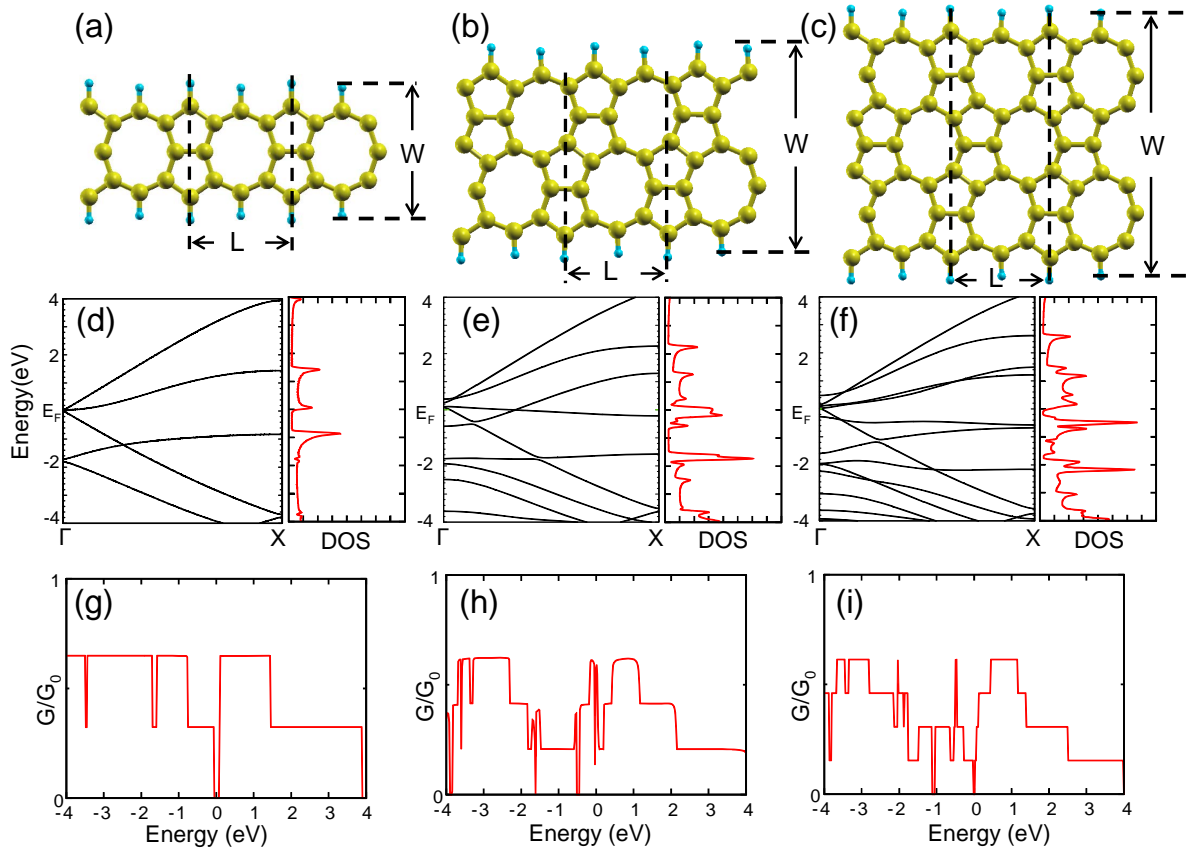


**Figure 2.** (Color online) Atomic structure, electronic band structure and transport properties of haeckelite nanoribbons passivated by hydrogen at the edge. Atomic structure of haeckelite nanoribbons with various width are shown in (a), (b), (c). The corresponding electronic band structure and density of states is shown in (d), (e), (f), and ballistic transport conductance  $G/G_0$  in (g), (h), (i). The density of state is given per atom.

the three h-NRs in units of the conductance quantum  $G_0$  is shown in Fig. 2(g-i). Of most interest is the presence or absence of a transport gap at  $E = 0$ , corresponding to carrier injection at  $E_F$ . As expected, the semiconducting nanoribbons depicted in Figs. 2(a) and 2(c), have also a finite transport gap, seen in Figs. 2(g) and 2(i). The metallic nanoribbon in Fig. 2(b) does not have a transport gap at  $E = 0$  according to Fig. 2(h).

Similar to graphene-based carbon nanotubes, we can construct 5-8 haeckelite-based nanotubes, and characterize them by the chiral index  $(n, m)$  in analogy to carbon nanotubes. We present the structure and electronic properties of two representative 5-8 haeckelite nanotubes, h-NT(0,2) and h-NT(2,0), in Fig. 3. Both the side and the end-on view of these nanotubes in Fig. 3(a,b) indicates that their optimum cross-section is not as round and their surface not as smooth as that of their graphitic counterparts, owing to the presence of 5- and 8-membered rings. We found the ultra-narrow h-NT(0,2) and h-NT(2,0) nanotubes to be stable, but highly strained. The stability of

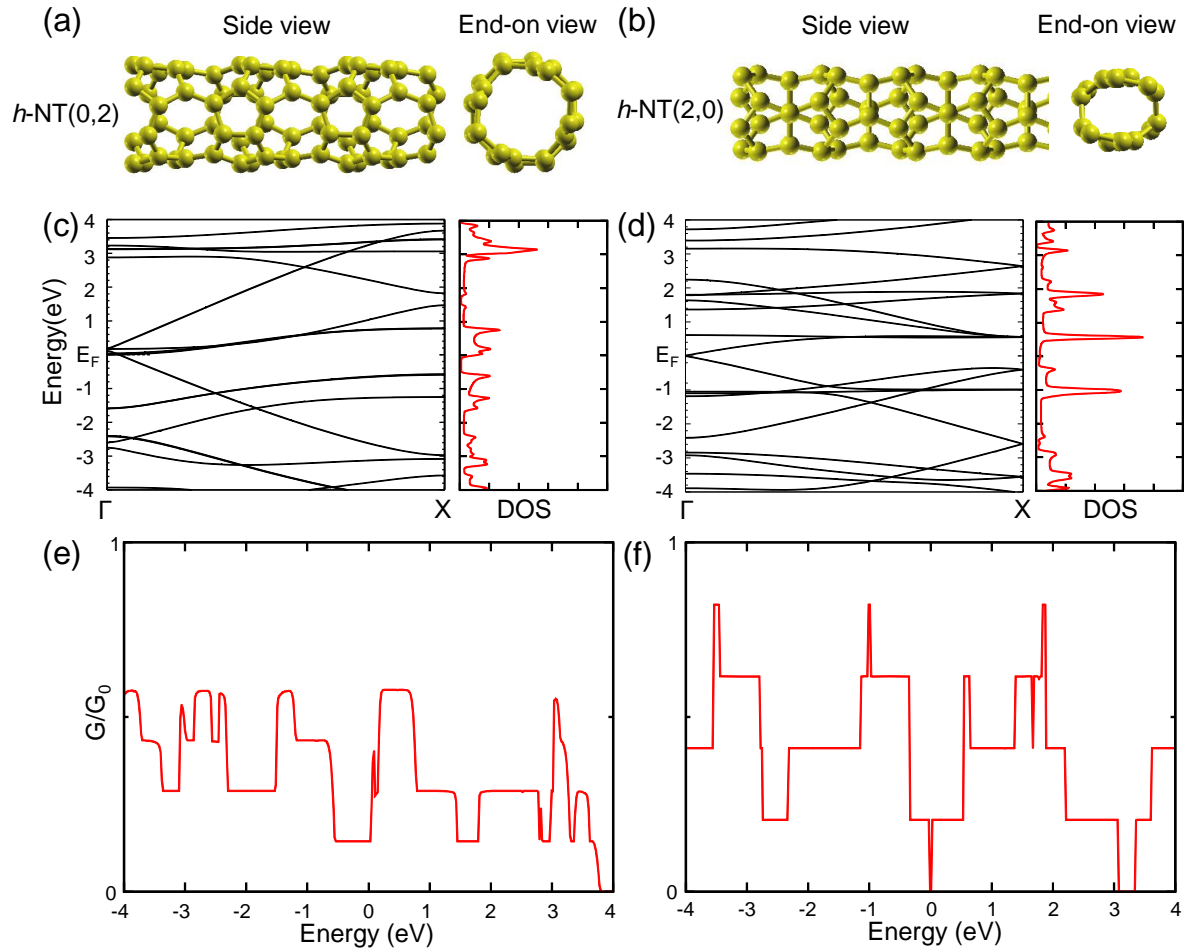


**Figure 3.** (Color online) Structural and electronic properties of haeckelite nanotubes. Atomic structure of (a) h-NT(0,2) and (b) h-NT(2,0) nanotubes. The length of the unit cells is denoted by  $L$  and the width by  $W$ . The corresponding electronic band structure and density of states is shown in (c), (d), and ballistic transport conductance  $G/G_0$  in (e), (f). The density of state is given per atom.

the narrower h-NT(2,0) is lower by 0.81 eV/atom and that of the wider h-NT(0,2) is lower by 0.45 eV/atom with respect to the planar haeckelite structure depicted in Fig. 1(a).

The electronic band structure and density of states of the h-NT(0,2) nanotube, shown in Fig. 3(c), indicates that h-NT(0,2) is metallic and has a non-zero density of states at the Fermi energy. As expected, also the calculated quantum conductance, shown in Fig. 3(e), indicates non-vanishing quantum conductance at  $E = 0$ . Quite different are the electronic structure and quantum conductance results for the h-NT(2,0) nanotube, shown in Fig. 3(d) and 3(f), which display a very small fundamental and transport gap of  $< 0.1$  eV. Unlike in graphene-based carbon nanotubes, there is no general rule to predict whether a given h-NT nanotube should be metallic or semiconducting.

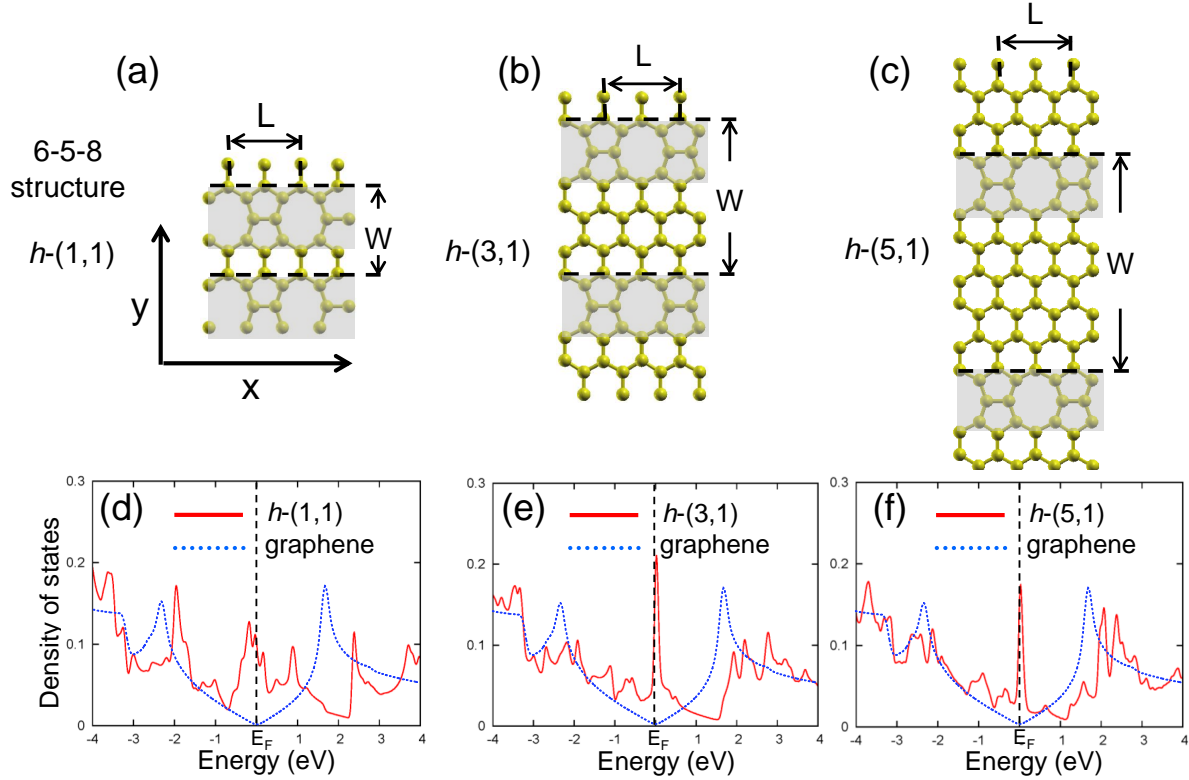


**Figure 4.** (Color online) Structure and electronic properties of hybrid haeckelite/graphene structures  $h-(n,m)$  consisting of graphene strips interconnected by 5-8 haeckelite strips, with  $n$  referring to the width of graphene and  $m$  to that of haeckelite. The upper panels depict the atomic structure of (a)  $h-(1,1)$ , (b)  $h-(3,1)$  and (c)  $h-(5,1)$  hybrid structures with  $m = 1$ . The corresponding electronic densities of states are shown in the lower panels (d), (e) and (f). The length of the unit cells is denoted by  $L$  and the width by  $W$ . The density of state is given per atom.

### 3.3. Hybrid haeckelite-graphene structures

As a model of haeckelite-like grain boundaries connecting graphene grains in polycrystalline graphene samples, we construct hybrid haeckelite-graphene structures consisting of strips of 5-8 h-NRs of various width inter-connecting bare zigzag graphene nanoribbons with different widths. The hybrid systems, identified as  $h-(n,m)$ , are characterized by the number  $m$  of 8-membered rings per unit cell and the number  $n$  of hexagonal rings across the width of the unit cell. We explored two families of hybrid structures with  $m = 1$  and  $m = 2$ , but different values of  $n$ . These studies let us explore how the density of 5-8 line defects should affect the electronic and transport properties of the hybrid structures.

The optimum atomic arrangement and electronic structure of  $h-(n, 1)$  hybrids, with  $n = 1, 3, 5$ , is shown in Fig. 4. We found all the structures to be metallic, as indicated by the peak in electronic densities of states at the Fermi energy in Figs. 4(d-f). The peak is associated with the 5-8 defects and decreases in strength with decreasing fraction of these defects in the structure, as the graphene strips become wider.



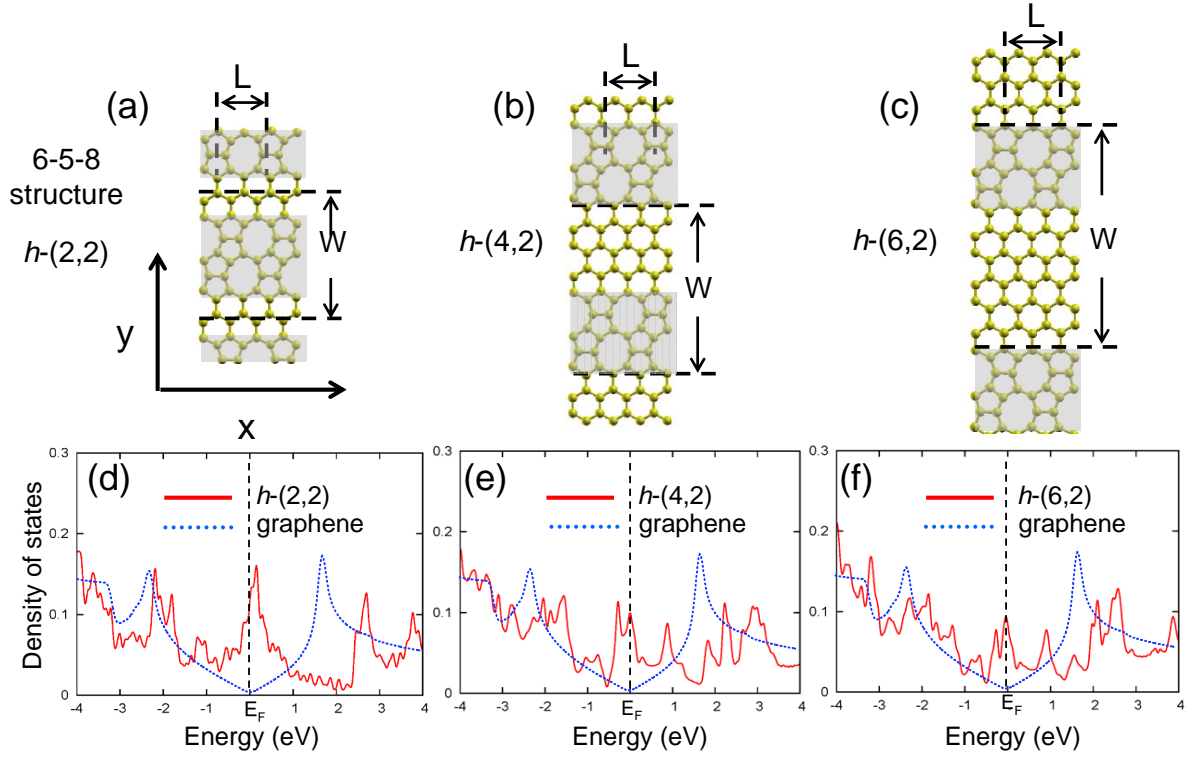


**Figure 5.** (Color online) Structure and electronic properties of hybrid haeckelite/graphene structures  $h-(n,m)$  consisting of graphene strips interconnected by 5-8 haeckelite strips, with  $n$  referring to the width of graphene and  $m$  to that of haeckelite. The upper panels depict the atomic structure of (a)  $h-(2,2)$ , (b)  $h-(4,2)$  and (c)  $h-(6,2)$  hybrid structures with  $m = 2$ . The corresponding electronic densities of states are shown in the lower panels (d), (e) and (f). The length of the unit cells is denoted by  $L$  and the width by  $W$ . The density of state is given per atom.

The corresponding results for  $h-(n, 2)$  hybrids, with wider haeckelite strips ( $m = 2$ ) and also wider graphene strips characterized by  $n = 2, 4, 6$ , are shown in Fig. 5. Similar to the  $m = 1$  family presented in Fig. 4, also the  $h-(n, 2)$  structures are all metallic, but the peak in the density of states peak near  $E_F$  does not appear as sharp as in the  $h-(n, 1)$  structures. Similar to  $h-(n, 1)$  hybrids, the effect of the defect line diminished with increasing  $n$ .

For the sake of illustration, we included the density of states of pristine graphene in the same energy range and observe that presence of 5-8 haeckelite line defects increases the density of states near the Fermi level, benefitting conductivity.

We note that the narrow haeckelite strips within the  $h-(n, 1)$  hybrid structures correspond to the free-standing, but hydrogen-passivated nanoribbon presented in Fig. 2(a). Similarly, also the wider haeckelite strips within the  $h-(n, 2)$  hybrid structures have a counterpart in the free-standing, but hydrogen-passivated nanoribbon presented in Fig. 2(b). Comparison between the density of states of the free-standing haeckelite nanoribbons in Fig. 2(d,e) and the densities of states in Figs. 4(d-f) and Figs. 5(d-f) indicates that the electronic structure of free-standing and embedded nanoribbons is



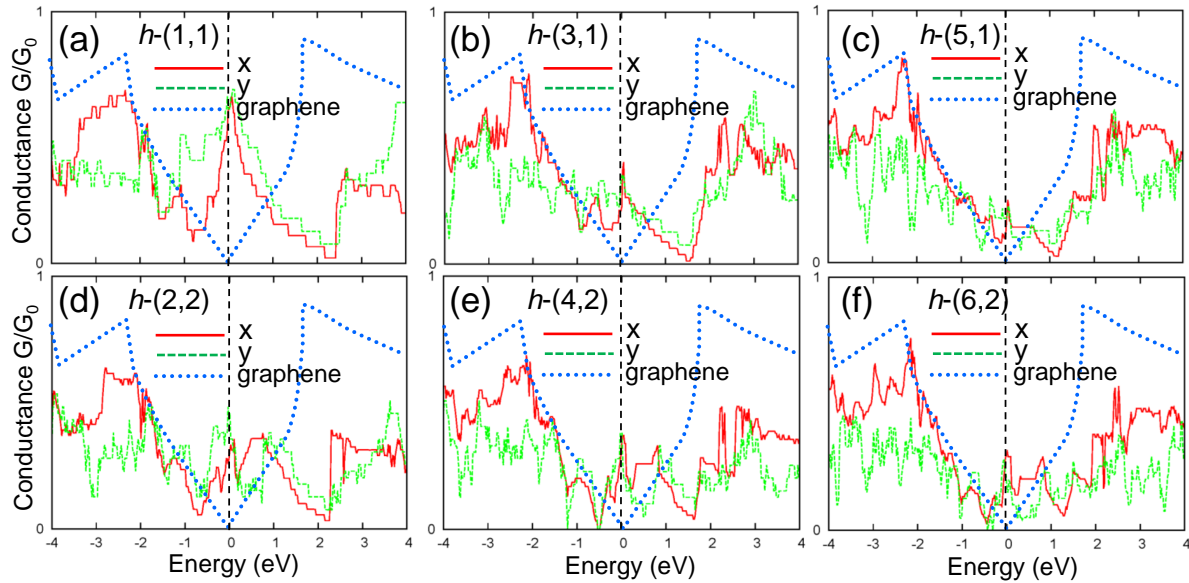


**Figure 6.** (Color online) Electronic conductance  $G$  of hybrid haeckelite/graphene structures  $h-(n,m)$  consisting of graphene strips interconnected by 5-8 haeckelite strips. Results are presented for (a)  $h-(1,1)$ , (b)  $h-(3,1)$ , (c)  $h-(5,1)$ , (d)  $h-(2,2)$ , (e)  $h-(4,2)$ , (f)  $h-(6,2)$  with different widths  $n$  of the graphene strips and  $m$  of the haeckelite strips. The structures and transport directions are defined in Figs. 4(a-c) and 5(a-c).  $G$  is normalized by the width of the unit cell normal to the transport direction.  $E = 0$  corresponds to carrier injection at  $E_F$ .

very different.

The increasing similarity of  $h-(n,m)$  structures with increasing width  $n$  of the graphene strips and defect-free graphene is also reflected in the quantum conductance of these systems, shown in Fig. 6. Unlike the density of states, quantum conductance is anisotropic. Especially for large values of  $n$ , transport along the defect lines will increasingly resemble that of graphene superposed with that of the conducting defect lines acting as quantum conductors or metal wires. We conclude that lines of non-hexagonal rings at grain boundaries in polycrystalline graphene should enhance the conductance of this system over pristine semimetallic graphene.

#### 4. Conclusions

In conclusion, we have combined *ab initio* density functional theory (DFT) structural studies with DFT-based nonequilibrium Green function calculations to study how the presence of non-hexagonal rings affects electronic transport in graphitic structures found in polycrystalline graphene. We found that infinite monolayers, finite-width nanoribbons and nanotubes formed of 5-8 haeckelite with only 5- and 8-membered rings are generally more conductive than their graphene-based counterparts. Presence of haeckelite defect lines in the perfect graphitic structure, a model of grain boundaries in CVD-grown graphene, increases the electronic conductivity and renders it highly anisotropic.

## Acknowledgments

The authors acknowledge financial support from the National Science Foundation Cooperative Agreement No. EEC-0832785, titled “NSEC: Center for High-rate Nanomanufacturing”. Computational resources have been provided by the Michigan State University High Performance Computing Center.

## References

- [1] Novoselov K S, Geim A K, Morozov S V, Jiang D, Zhang Y, Dubonos S V, Grigorieva I V and Firsov A A 2004 *Science* **306** 666–669 URL <http://dx.doi.org/10.1126/science.1102896>
- [2] Bolotin K, Sikes K, Jiang Z, Klima M, Fudenberg G, Hone J, Kim P and Stormer H 2008 *Solid State Commun.* **146** 351–355 URL <http://www.sciencedirect.com/science/article/pii/S0038109808001178>
- [3] Novoselov K S, Jiang D, Schedin F, Booth T J, Khotkevich V V, Morozov S V and Geim A K 2005 *Proc. Natl. Acad. Sci. U.S.A* **102** 10451–10453
- [4] Kim K S, Zhao Y, Jang H, Lee S Y, Kim J M, Kim K S, Ahn J H, Kim P, Choi J Y and Hong B H 2009 *Nano Lett.* **457** 706 URL <http://dx.doi.org/10.1038/nature07719>
- [5] Reina A, Jia X, Ho J, Nezich D, Son H, Bulovic V, Dresselhaus M S and Kong J 2009 *Nano Lett.* **9** 30 URL <http://dx.doi.org/10.1021/nl801827v>
- [6] Kim K S, Zhao Y, Jang H, Lee S Y, Kim J M, Kim K S, Ahn J H, Kim P, Choi J Y and Hong B H 2009 *Nature* **457**(7230) 706–710 URL <http://dx.doi.org/10.1038/nature07719>
- [7] Li X, Cai W, An J, Kim S, Nah J, Yang D, Piner R, Velamakanni A, Jung I, Tutuc E, Banerjee S K, Colombo L and Ruoff R S 2009 *Science* **324** 1312–1314 URL <http://www.sciencemag.org/content/324/5932/1312.abstract>
- [8] Crespi V H, Benedict L X, Cohen M L and Louie S G 1996 *Phys. Rev. B* **53**(20) R13303–R13305
- [9] Terrones H, Terrones M, Hernández E, Grobert N, Charlier J C and Ajayan P M 2000 *Phys. Rev. Lett.* **84**(8) 1716–1719
- [10] Wang X Q, Li H D and Wang J T 2013 *Phys. Chem. Chem. Phys.* **15**(6) 2024–2030
- [11] Lusk M T and Carr L D 2008 *Phys. Rev. Lett.* **100**(17) 175503
- [12] Appelhans D J, Lin Z and Lusk M T 2010 *Phys. Rev. B* **82**(7) 073410
- [13] Appelhans D J, Carr L D and Lusk M T 2010 *New J. Phys.* **12** 125006
- [14] Huang P Y, Ruiz-Vargas C S, van der Zande A M, Whitney W S, Levendorf M P, Kevek J W, Garg S, Alden J S, Hustedt C J, Zhu Y, Park J, McEuen P L and Muller D A 2011 *Nature* **469** 389–392 URL <http://dx.doi.org/10.1038/nature09718>
- [15] Fthenakis Z G, Zhu Z and Tománek D 2014 *Phys. Rev. B* **89**(12) 125421
- [16] Botello-Méndez A R, Cruz-Silva E, López-Urías F, Sumpter B G, Meunier V, Terrones M and Terrones H 2009 *ACS Nano* **3** 3606–3612 pMID: 19863086
- [17] Rocquefelte X, Rignanese G M, Meunier V, Terrones H, Terrones M and Charlier J C 2004 *Nano Lett.* **4** 805–810
- [18] Lisenkov S, Andriotis A N, Ponomareva I and Menon M 2005 *Phys. Rev. B* **72**(11) 113401
- [19] Li Y F, Li B R and Zhang H L 2008 *J. Phys. Cond. Matter* **20** 415207
- [20] Popović Z, Milošević I and Damnjanović M 2011 *Mat. Sci. Eng. B* **176** 494–496
- [21] Lahiri J, Lin Y, Bozkurt P, Oleynik I I and Batzill M 2010 *Nat. Nanotechnol.* **5**(5) 326–329
- [22] Huang P Y, Ruiz-Vargas C S, van der Zande A M, Whitney W S, Levendorf M P, Kevek J W, Garg S, Alden J S, Hustedt C J, Zhu Y, Park J, McEuen P L and Muller D A 2011 *Nature* **469** 389–392
- [23] Eder F R, Kotakoski J, Kaiser U and Meyer J C 2014 *Sci. Rep.* **4** 4060
- [24] Zan R, Ramasse Q M, Bangert U and Novoselov K S 2012 *Nano Lett.* **12** 3936–3940
- [25] Wang Y, Page A J, Nishimoto Y, Qian H J, Morokuma K and Irlé S 2011 *J. Am. Chem. Soc.* **133**

18837–18842 (Preprint <http://dx.doi.org/10.1021/ja2064654>) URL <http://dx.doi.org/10.1021/ja2064654>

- [26] Enyashin A N and Ivanovskii A L 2011 *phys. stat. sol. (b)* **248** 1879–1883 ISSN 1521-3951
- [27] Su C, Jiang H and Feng J 2013 *Phys. Rev. B* **87**(7) 075453
- [28] Sheng X L, Cui H J, Ye F, Yan Q B, Zheng Q R and Su G 2012 *J. Appl. Phys.* **112** 074315
- [29] Liu Y, Wang G, Huang Q, Guo L and Chen X 2012 *Phys. Rev. Lett.* **108** 225505
- [30] Artacho E, Anglada E, Dieguez O, Gale J D, Garcia A, Junquera J, Martin R M, Ordejon P, Pruneda J M, Sanchez-Portal D and Soler J M 2008 *J. Phys. Cond. Matter* **20** 064208
- [31] Ceperley D M and Alder B J 1980 *Phys. Rev. Lett.* **45**(7) 566–569
- [32] Perdew J P and Zunger A 1981 *Phys. Rev. B* **23**(10) 5048–5079
- [33] Troullier N and Martins J L 1991 *Phys. Rev. B* **43** 1993
- [34] Monkhorst H J and Pack J D 1976 *Phys. Rev. B* **13**(12) 5188–5192
- [35] Hestenes M R and Stiefel E 1952 *J. Res. Natl. Bur. Stand.* **49** 409–436
- [36] Brandbyge M, Mozos J L, Ordejón P, Taylor J and Stokbro K 2002 *Phys. Rev. B* **65**(16) 165401